Supporting Information

Capabilities of Single Particle Inductively Coupled Plasma Mass Spectrometry for the Size Measurement of Nanoparticles: A Case Study on Gold Nanoparticles

Jingyu Liu[1, 2, ǂ], Karen E. Murphy[1, ǂ], Robert I. MacCuspie[2^], Michael R. Winchester[1, *]

[1]Chemical Sciences Division, [2] Materials Measurement Science Division, Material Measurement Laboratory, National Institute of Standards and Technology, Gaithersburg, Maryland 20899, United States

ǂ These authors contributed equally to this work

^ Current Address: Florida Polytechnic University, Nanotechnology Program, 439 S. Florida Ave., Suite 300, Lakeland, FL, USA 33801

*Corresponding author phone: 301-975-3886; Fax: 301-869-0413; e-mail: mwinchester@nist.gov

Table of Contents

Figure S9. Size distribution histograms for a mixed suspension containing AuNPs from 20 nm to 200 nm measured by spICP-MS under standard and reduced sensitivity conditions.

Figure S10. Overlaid size distribution histograms for a mixed suspension containing AuNPs from 20 nm to 200 nm measured by spICP-MS under standard and reduced sensitivity conditions.

Table S1. Probabilities calculated to justify split particle correction.

Table S2. Calculated probability of particle coincidence for different t_{dwell}.

Table S3. spICP-MS size measurements for 60 nm to 200 nm AuNPs under different instrument operating conditions after correction of split pulses and false positives.

Calculation of ICP-MS sensitivity

For a solution containing an analyte of mass concentration C (μg L^{-1}), the mass (m, μg) of the analyte that enters the plasma during a given dwell time (t_{dwell}, ms) is calculated by[1]:

$$m = C \times q_{liq} \times t_{dwell} \times \eta_n$$

where q_{liq} (L ms^{-1}) is the sample uptake rate and η_n is the transport efficiency (i.e., the fraction of the nebulized solution that is introduced into the plasma). This relationship can be used to convert the concentration based calibration curve to a mass based calibration curve, whose slope gives the sensitivity (counts μg^{-1}) of the ICP-MS instrument. Figure S1 shows an example of calculating the instrument sensitivity from dissolved Au standards.

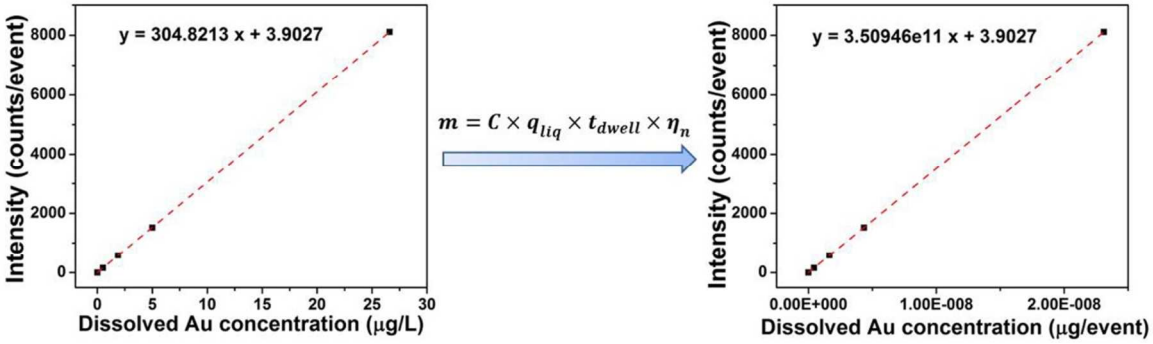

Figure S1. Determination of instrument sensitivity from dissolved Au standards. The instrument sensitivity is derived from the dissolved Au standard calibration (left) by converting the concentration units from μg L^{-1} to μg $event^{-1}$ (right). The obtained sensitivity for ^{197}Au is 3.51×10^{11} counts μg^{-1} Au. "Event" is equivalent to the dwell time and is used in this context to be commensurate with the introduction of a single nanoparticle into the plasma. The dots represent experimental data and the dashed lines give the linear fits of intensity vs. dissolved Au concentration.

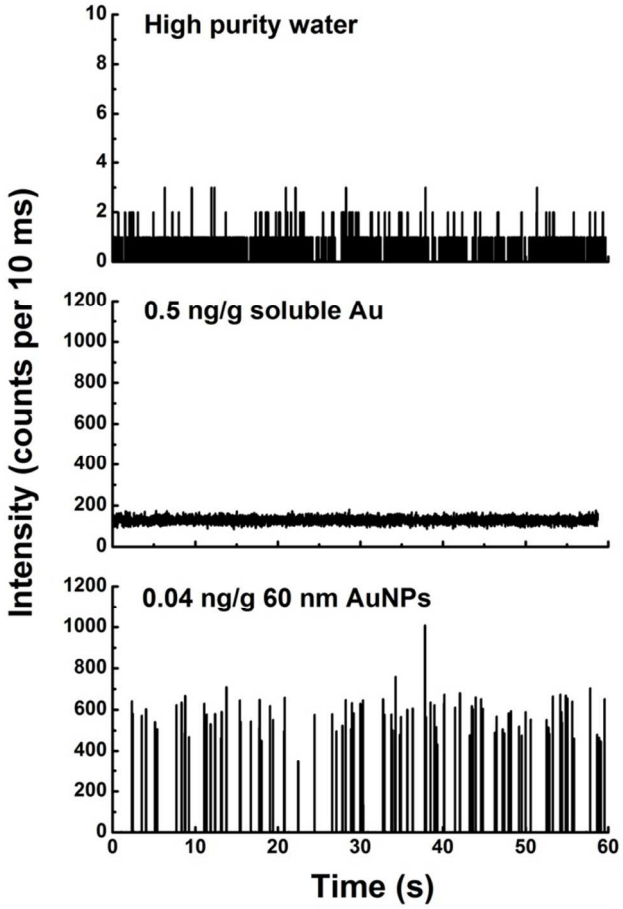

Figure S2. Time resolved spICP-MS measurements (^{197}Au) of high purity water, 0.5 ng g^{-1} dissolved Au in thiourea solution, and 0.04 ng g^{-1} (2.5×10^7 L^{-1}) 60 nm AuNPs (NIST RM 8013) in water. Dwell time: 10 ms.

Use of Poisson statistics to justify split particle correction

The Poisson distribution is a distribution of discrete events that occur in a fixed interval of time with a known average rate and independently of the time since the last event. In spICP-MS measurement, the particles arrive randomly at the plasma. The probability, $P(n)$, of recording a signal from n nanoparticles within a given time interval t can be estimated by the Poisson distribution[2]:

$$P(n) = \frac{\lambda^n}{n!} e^{-\lambda}$$

where λ is the average number of particles that enter the plasma during time t.

We first use the Poisson distribution to estimate the probability of detecting a single particle event that is split between two adjacent measurement windows. The approximation is given by the Poisson equation for $n = 1$, modified by the ratio of the width of a nanoparticle signal pulse t_{pulse} to t_{dwell}:

$$P_{split} = \frac{P(1)}{\left(1 - P(0)\right)}\left(\frac{t_{pulse}}{t_{dwell}}\right) = \frac{t_{pulse}\lambda e^{-\lambda}}{t_{dwell}(1 - e^{-\lambda})}$$

Values for this probability estimation are presented in Table S1 for different t_{dwell}, given our typical experimental conditions (nanoparticle concentration, sample uptake rate and transport efficiency) and the fact that we observed a t_{pulse} of about 0.4 ms under those conditions.

Next, we estimate the probability of observing two nanoparticle pulses in adjacent measurement windows. Considering the side by side particle events in two adjacent t_{dwell} windows to be a case of registering two particles within $t = 2t_{dwell}$, and the fact that during $2t_{dwell}$ the probabilities of these two particles appearing within the same t_{dwell} and separately in each t_{dwell} are both 0.5, the probability of detecting side by side particle events for a given t_{dwell} among all the observed particle events is given by:

$$P_{adjacent} = \frac{\left(\frac{P_2(2)}{2}\right)}{\left(1 - P_1(0)\right)} = \lambda_1^2 e^{-\lambda_2}/(1 - e^{-\lambda_1})$$

where P_1 and P_2 are the probabilities of recording a signal from n particles within a time interval of t_{dwell} and $2t_{dwell}$, respectively. The parameters, λ_1 and λ_2, are the mean number of particles that enter the plasma during t_{dwell} and $2t_{dwell}$, respectively, where $\lambda_2 = 2\lambda_1$. The estimated probability of detecting two consecutive particle events in two adjacent measurement windows under the typical experimental conditions as a function of t_{dwell} is also given in Table S1.

The most important data in Table S1 are in the last column, which presents the ratios of the two probability values for different values of t_{dwell}. These ratios show that particle events split between two adjacent measurement windows are much more likely than side by side particles in adjacent measurement windows for short t_{dwell}. The ratio decreases dramatically as t_{dwell} is lengthened, but remains greater than or nearly equal to 1 for dwell times up to 15 ms. For t_{dwell} = 20 ms, split particle events appear to be less probable than side by side events.

The implication is that summing signal intensities in adjacent measurement windows can be used effectively to correct for split particles for dwell times up to 5 ms, with minimal errors introduced by accidentally summing signals caused by two adjacent particles. When this sort of split particle correction is used with longer dwell times, precautions should be taken to avoid such errors. When the sample is known to be monodisperse, simply avoiding summing signals that are approximately equal to each other and the expected intensity of a single particle is an effective strategy and was used in this work. However, if the sample has an unknown particle size distribution, this would not be possible and it would be prudent to use split particle correction only with short dwell times.

Table S1. Probabilities for different dwell times of detecting a single nanoparticle pulse split between two adjacent measurement windows and of detecting two nanoparticles in adjacent measurement windows, along with the ratios of these two probability values. Nanoparticle flux was assumed to be 135 min^{-1}, based on a typical particle number concentration of 2.5 $\times 10^7$ L^{-1}, sample uptake rate of 0.18 mL min^{-1} and transport efficiency of 3 %. The signal pulse caused by a nanoparticle was assumed to be 0.4 ms, as observed in this work.

Dwell time (ms)	P_{split} (%)	$P_{adjacent}$ (%)	$P_{split}/P_{adjacent}$
1	40	0.22	178
5	8.0	1.1	7.2
10	4.0	2.2	1.8
15	2.6	3.2	0.82
20	2.0	4.2	0.46

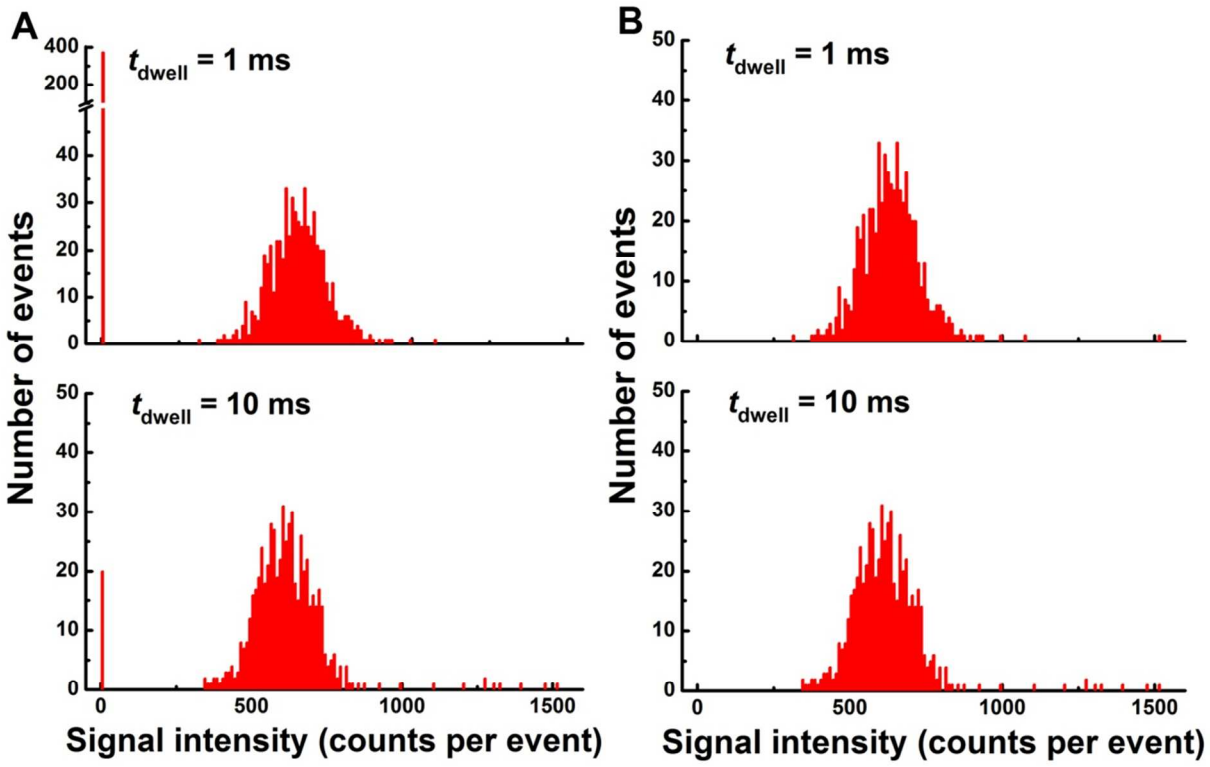

Figure S3. Intensity histograms for 60 nm AuNPs (NIST RM 8013) measured with t_{dwell} of 1 ms and 10 ms before (A) and after (B) elimination of false positives. Data show only particle signals distinguished from the background using 5σ criterion and after correction of split pulses. The events with intensity < 5 counts event^{-1} were identified as false positives and removed from intensity histograms in (A). The results summarize 6 replicates of 60 s runs. Bin size is 10 counts event^{-1}.

Use of Poisson distribution to estimate the probability of particle coincidence

For a given particle number concentration, N_P (mL^{-1}), the particle flux, $f(_P)$ (min^{-1}), can be calculated by:

$$f(_P) = N_P \times q_{liq} \times \eta_n$$

where q_{liq} is the sample flow rate (mL min^{-1}), and η_n is the transport efficiency.

Based on the Poisson distribution, the probability of recording a signal from n nanoparticles within a given t_{dwell} can be calculated by:

$$P(n) = \frac{\lambda^n}{n!} e^{-\lambda}$$

where λ, the average number of particles that enter the plasma during time t_{dwell}, is calculated by $\lambda = f(_P) \times t_{dwell}$. The probability of getting zero particles per event (P(0)), one particle per event (P(1)), and more than one particle per event (P(>1)) can then be calculated accordingly.

Table S2. Calculated probability of particle coincidence for different t_{dwell}

t_{dwell} (ms)	P(0) %	P(1) %	P(>1) %	Percentage of coincidence P(>1)/((P(1)+(P(>1))*100
1	99.78	0.22	0.00	0.11
5	98.88	1.11	0.01	0.56
10	97.78	2.20	0.02	1.12
15	96.68	3.26	0.06	1.68
20	95.60	4.30	0.10	2.23

* Nanoparticle flux is estimated using typical particle number concentration of 2.5 ×10^7 L^{-1}, sample uptake rate of 0.18 mL min^{-1}, and transport efficiency of 3 %.

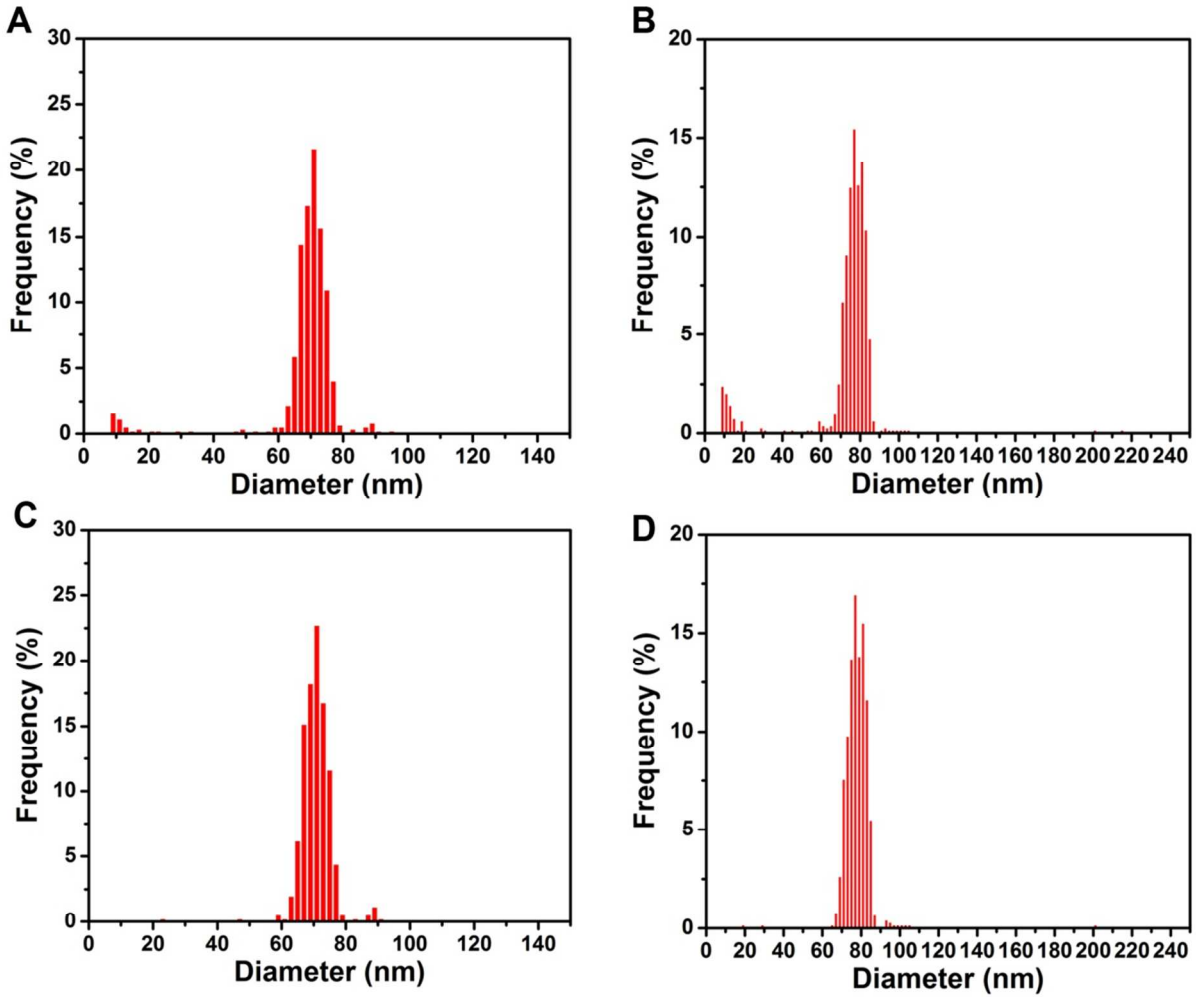

Figure S4. Particle size distribution of (A, C) 80 nm and (B, D) 100 nm AuNPs determined by spICP-MS under the standard sensitivity condition. (A) and (B) were calculated from as-recorded single particle events, while (C) and (D) were derived after data correction for split pulses and false positives, showing elimination of split particle and false positive events after data correction. Measurements were conducted using t_{dwell} of 10 ms and acquisition time of 360 s.

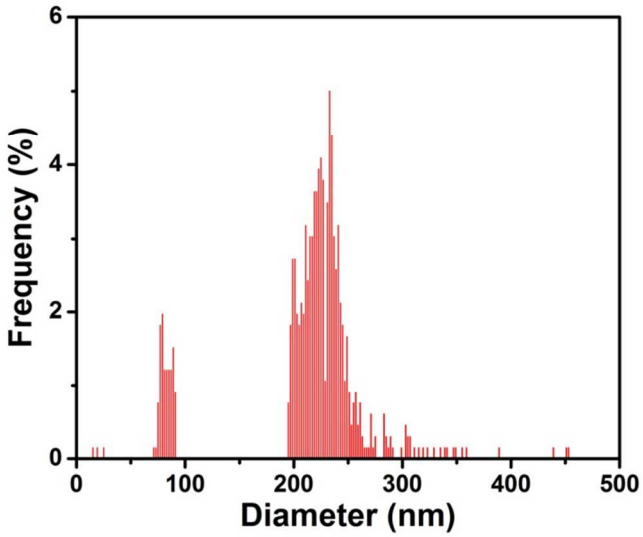

Figure S5. Particle size distribution of 200 nm AuNPs determined by spICP-MS under the standard sensitivity condition after correction of split particle events and false positives. Measurements were conducted using t_{dwell} of 10 ms and acquisition time of 360 s.

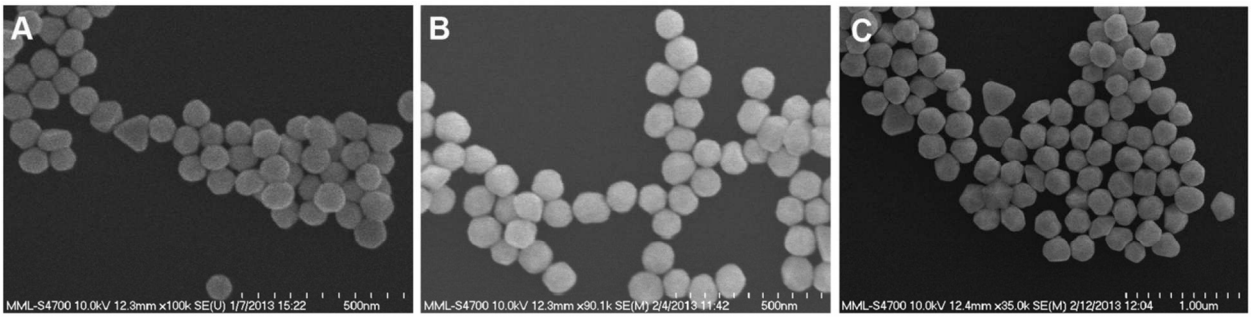

Figure S6. SEM images of (A) 80 nm, (B) 100 nm, and (C) 200 nm AuNPs.

Table S3. spICP-MS size measurements for 60 nm to 200 nm AuNPs under different instrument operating conditions after correction of split pulses and false positives.

Average diameter (nm)		60 nm	80 nm	100 nm	200 nm
	TEM[1]	56.0	80.0	99.6	203.6
spICP-MS[2]	Condition 1: Standard mode	55.9 ± 3.3	70.8 ± 4.7	78.0 ± 7.1	212.4 ± 58.0 [3]
	Condition 2: Low extraction voltage	55.0 ± 7.9	82.3 ± 6.5	103.2 ± 7.8	196.9 ± 11.9
	Condition 3: Collision cell/KED	54.8 ± 8.7	82.5 ± 8.3	105.2 ± 9.0	205.8 ± 14.0
	Condition 4: High resolution	54.6 ± 8.1	80.4 ± 8.4	101.0 ± 11.0	201.7 ± 17.8
	Condition 5: Low extraction voltage + Collision cell/KED	55.0 ± 7.8	82.2 ± 7.5	103.6 ± 8.7	204.5 ± 12.5

[1] The mean TEM diameters are reported by the vendors

[2] The average diameter and uncertainty (one standard deviation) are calculated from the size distribution measured by spICP-MS using t_{dwell} of 10 ms and acquisition time of 360 s for Condition 1, and acquisition time of 200 s for Conditions 2 - 5. Particle intensity data were corrected for split pulses and false positives.

[3] Bimodal size distribution, as shown in Fig. S5.

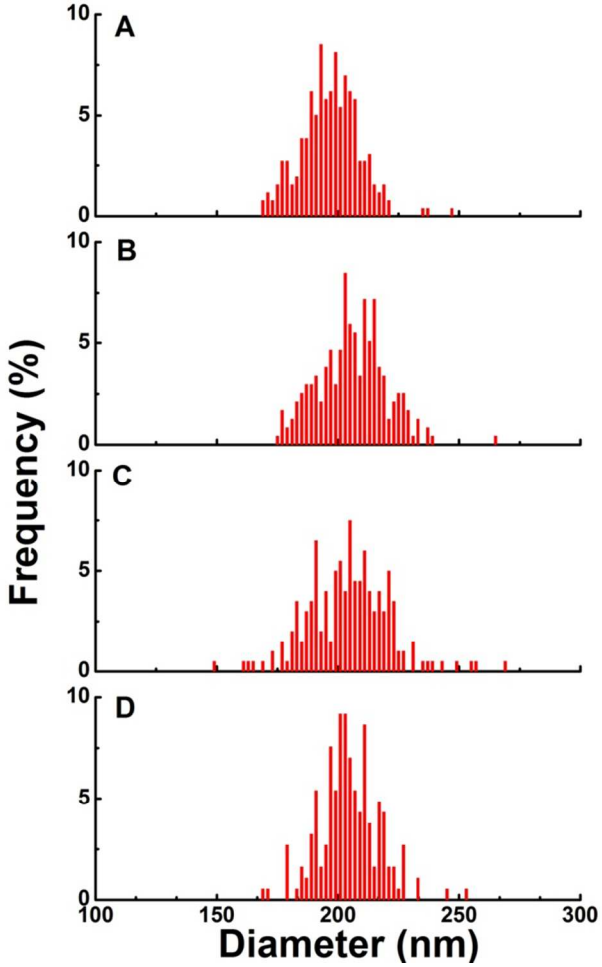

Figure S7. Size distribution histograms for 200 nm AuNPs measured by spICP-MS under different operating conditions after correction of split pulses and false positives: (A) Condition 2, low extraction voltage; (B) Condition 3, collision cell/KED; (C) Condition 4, high resolution; and (D) Condition 5, low extraction voltage + collision cell/KED. Single particle ICP-MS used t_{dwell} of 10 ms and acquisition time of 200 s. Bin size is 2 nm.

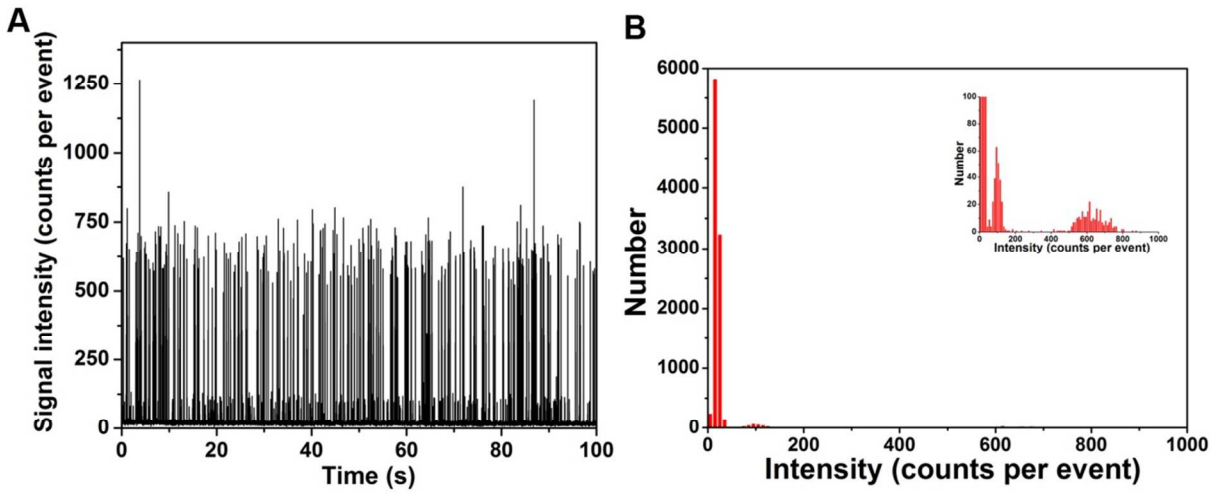

Figure S8. spICP-MS measurement (^{197}Au) of a mixture containing 0.050 ng g^{-1} soluble Au, 0.005 ng g^{-1} (2.45 × 10^{7} L^{-1}) 30 nm AuNPs (NIST RM 8012), and 0.043 ng g^{-1} (2.44 × 10^{7} L^{-1}) 60 nm AuNPs (NIST RM 8013). (A) Time resolved intensity profile, and (B) Intensity distribution histogram, the insert shows intensity peaks for 30 nm and 60 nm AuNPs. Experiment used t_{dwell} of 10 ms under standard condition.

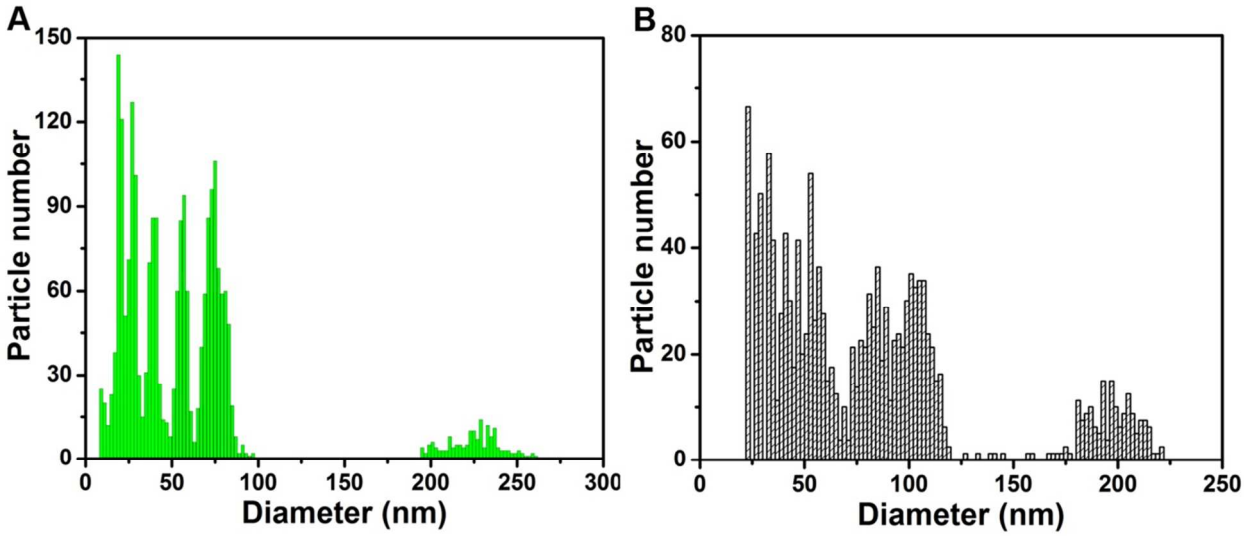

Figure S9. Size distribution histograms for a mixed suspension containing AuNPs from 20 nm to 200 nm measured by spICP-MS at (A) standard mode (Condition 1, Table 1) and (B) reduced sensitivity mode (Condition 2, Table 1). The suspension contains AuNPs of 20 nm, 30 nm, 40 nm, 60 nm, 80 nm, 100 nm and 200 nm, each with number concentration of 1.2 × 10^{7} L^{-1}. It was measured by spICP-MS using t_{dwell} of 10 ms and acquisition time of 300 s.

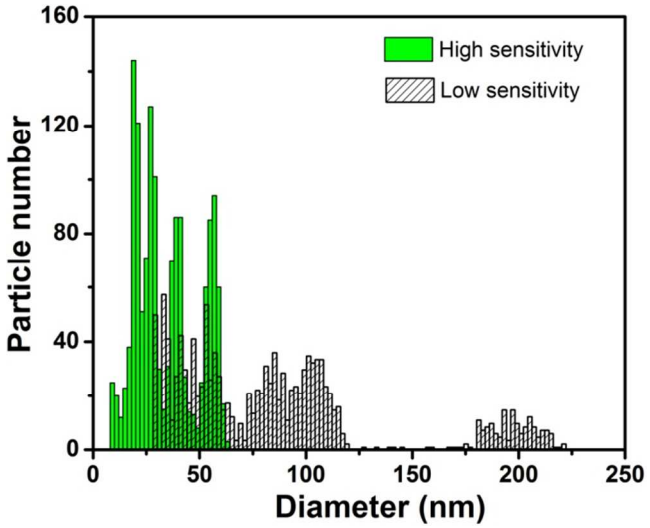

Figure S10. Overlaid size distribution histograms for a mixed suspension containing AuNPs from 20 nm to 200 nm measured by spICP-MS at standard mode (Condition 1, Table 1) and reduced sensitivity mode (Condition 2, Table 1). The suspension contains AuNPs of 20 nm, 30 nm, 40 nm, 60 nm, 80 nm, 100 nm and 200 nm, each with number concentration of 1.2×10^7 L^{-1}. The particles with ICP-MS intensity greater than 1000 counts $event^{-1}$ or less than 2.5 counts $event^{-1}$ were removed from Fig. S6, and the two diagrams were overlaid to show the match of 60 nm AuNPs.

REFERENCES:

1. Pace, H. E.; Rogers, N. J.; Jarolimek, C.; Coleman, V. A.; Higgins, C. P.; Ranville, J. F. *Anal. Chem.* **2011**, *83*, 9361-9369.

2. Olesik, J. W.; Gray, P. J. *J. Anal. At. Spectrom.* **2012**, *27*, 1143-1155.